Impact toughness improvement of high strength aluminium alloy by intrinsic and extrinsic fracture mechanisms via hot roll bonding

C.M. Cepeda-Jiménez[a]*, J.M. García-Infanta[a], M. Pozuelo[b], O.A. Ruano[a], F. Carreño[a]

[a]*Department of Physical Metallurgy, CENIM, CSIC, Av. Gregorio del Amo 8, 28040 Madrid, Spain*

[b]*Department of Materials Science and Engineering, 6531-G Boelter Hall, University of California, Los Angeles, CA 90095-1595, USA*

A multilayer aluminium laminate comprising ten layers of Al-Zn-Mg-Cu alloy (82 vol.%) and nine layers of pure aluminium (18 vol.%) has been processed by hot rolling. The rolled laminate was characterized by electron backscattering diffraction, Charpy impact and shear tests. The multilayer laminate showed an outstanding Charpy impact toughness, being eighteen times higher than that for the as-received Al-Zn-Mg-Cu alloy. Damage tolerance improvement was due to the high volume fraction of the high strength aluminium and extrinsic fracture mechanisms.

Keywords: Aluminium alloys; Multilayer; Interfaces; Impact behaviour; Delamination.

*Corresponding author. Tel.: +34 91 5538900; fax: +34 91 5347425.
E-mail address: cm.cepeda@cenim.csic.es (C.M. Cepeda-Jiménez)

The highest strengths attained in wrought aluminium alloys correspond to the Al-Zn-Mg-Cu alloys (7xxx-serie) [1]. However, these heat-treatable aluminium alloys exhibit low fracture toughness, which limits their extensive application.

In recent years, metallic multilayer composites have received attention due to their striking characteristics [2,3]. In particular, from a mechanical point of view multilayer materials are able to reach an optimized combination of strength and toughness [4]. Hot rolling is capable of obtaining good bonds between metallic layers improving toughness and refining the microstructure [5-9]. The interfaces that may delaminate are responsible for the high fracture resistance of the multilayer materials, and contribute to increase the extrinsic toughening by different mechanisms [10]. Multilayer laminates based in aluminium alloys have been developed by hot roll-bonding, resulting in materials of improved impact toughness [11]. In this previous

work, the aim was to optimize the rolling strain in two multilayer laminates with similar volume fraction of high strength Al 7075 and Al 1050.

In the present study, a hot-rolled aluminium multilayer laminate based mainly in Al 7075 alloy (82% volume fraction) with high strength and outstanding impact toughness has been processed. Since Al 7075 alloy exhibits a high work hardening rate, which may be problematic during processing, thinner Al 1050 layers than in previous works [10, 11] have been placed among the Al 7075 to facilitate bonding between sheets and to contribute to the intrinsic toughness. Therefore, the objective of this work is to improve the intrinsic and extrinsic fracture mechanisms, which are involved in the improvement of impact toughness of Al 7075. Hence, a high strength multilayer material based on alternated layers of Al 7075 (82% volume fraction) and Al 1050 (18% volume fraction) has been processed and characterized.

The aluminium alloys used were rolled Al 7075-T6 alloy (termed "D") of 2 mm in thickness and foils of Al 1050-H24 (termed "H") of 0.5 mm in thickness. The main alloying elements of the Al 7075 are Zn (5.95 wt.%), Mg (2.52 wt.%) and Cu (1.36 wt.%). Ten Al 7075 layers (D) and nine Al 1050 (H) layers were stacked alternately, making up a bundle of 24.5 mm in thickness, 60 mm in width and 150 mm in length and referenced as ADH19, with a ratio of Al 7075 to Al 1050 in volume of 82:18. The stacked multilayer material was welded by Tungsten Inert Gas (TIG) and then hot-rolled at 465 ºC in four series of four passes of about 4-8% reduction per pass, corresponding to an equivalent true strain of ε=0.85 (von Mises criterion) (reduction of 2.1:1). The diameter of the rolls was 130 mm and the rolling speed was 346 mm/s. The laminate was rolled parallel to the rolling direction of the as-received sheets. After hot rolling, a T6 heat treatment was carried out [11]. The resulting laminate was a plate of thickness about 11.5 mm, length 350 mm and width 60 mm. The final thickness of the Al 7075 layers in the ADH19 laminate was ~990 μm and that of the Al 1050 layers was ~270 μm.

The microstructure in the normal direction (ND)-rolling direction (RD) sections of the as-received materials and the laminate material was observed by scanning electron microscopy (SEM), using a JEOL JSM 6500F equipment with field emission gun. Microtexture information was obtained by electron backscattering diffraction technique (EBSD), operating with an accelerating voltage and working distance of 20keV and 15mm, respectively. The data processing was carried out using HKL Channel 5 software. Orientation mapping was performed with a step size between 0.3 and 0.6 μm depending on the magnification. A low angle grain boundary (LAB) was defined by a misorientation between adjacent grains of $2º<\theta<15º$, and a high angle grain boundary (HAB) was defined by $\theta>15º$. HABs and LABs are shown as black and white lines

respectively on the maps. The laminate impact toughness was measured by Charpy tests on a pendulum impact tester with a maximum capacity of 294 J. Two mm V-notched Charpy type testing samples were machined with 10x10x55 mm^3 dimensions from the as-received monolithic alloys and the roll-bonding laminate, which were tested in the crack arrester orientation. The rolled microstructure in the as-received aluminium materials, with elongated grains in the rolling direction, permits to distinguish two different orientations. Thus, for the as-received materials, in the so-called crack arrester orientation the notch tip is parallel to the plane and rolling directions. For the laminate materials, in the crack arrester orientation, the crack is forced to pass through each layer sequentially, and it is the natural configuration for an aluminium panel in an airplane. Selected fractured specimens were examined by SEM to evaluate deformation micromechanisms during crack propagation. The interface mechanical properties were measured by shear tests in a *Servosis* universal test machine at a cross-head rate of 0.005 mm/s, using specimens of ~ 10x10x3 mm^3 dimensions. The shear stress, τ, and the shear strain, γ, are given by the expressions $\tau=p/ae$; $\gamma=tan(\alpha)=d/l_{gap}$ [12], where a and e are the initial width and thickness of the sample respectively, p is the force applied on the sample, d is the midspan displacement of the sample, α is the shear angle and l_{gap} is the span length between the supports and the mobile punch, corresponding to 0.35 mm in this study. A scheme of the shear test performed was shown elsewhere [13].

Figure 1a shows the microstructure of the as-received Al 1050-H24. It presents an equiaxed (sub)grain structure with an average (sub)grain size of 2-3 μm. The as-received Al 7075-T6 (**Fig 1b**) shows large grains (20-30 μm) that are elongated and flattened parallel to the rolling direction. Additionally, randomly distributed iron-rich intermetallic particles were observed in both as-received materials. The EBSD map of the as-received Al 1050 carried out at low magnification (**Fig 1c**) shows a bimodal microstructure, highlighting a main lamellar structure composed of large grains elongated in the rolling direction containing fine subgrains (2-3 μm). Furthermore, small grains aggregates are observed along with the elongated grains. The EBSD map has been colour coded according to the inverse pole figure (IPF) shown in the inset, and the colours represent the crystallographic orientations parallel to ND. Thus, the spacing between HABs on the as-received Al 1050 presents a bimodal distribution with large grains 10-15 μm in thickness and small grains 2-3μm in thickness. On the other hand, the HAB spacing in the normal direction (ND) for the as-received Al 7075 was about 5.8 μm (**Fig 1d**). The 111 pole figure corresponding to the as-received Al 1050 (**Fig 1c**) shows a β-fibre ideal texture in rolled fcc metals [14]. The as-received 7075 material is weakly textured, slightly highlighting the Cube component ({001}<100>), which is

associated with partially recrystallized structures [15]. In general, the Al 7075 presents grains of a wide range of orientations (**Fig 1d**).

After rolling, the Al 7075 (D) in the ADH19-T6 laminate presents a RD-aligned lamellar microstructure separated by HABs (black lines) (**Fig. 2a** at low magnification, **and 2b** at higher magnification). **Figure 2a** shows the EBSD map of the ADH19-T6 laminate, containing alternating layers of large grains in the Al 1050 layers (H) and smaller "pancake" grains in the Al 7075 layers (D).

Figure 2 shows the reduction of HAB spacing in the Al 7075 to a value of about 3.8 μm. In addition, we can observe a typical β-fibre rolling texture, comprising variants of ideal orientation components {112}<111> (copper), {123}<634> (S3) and {110}<112> (Brass) in the Al 7075 layer (D) (**Fig 2b**) [15]. The Al 7075 alloy presents a finer microstructure in the ADH19-T6 laminate than in the as-received material (**Fig 1d**). As expected, high temperature roll bonding refines the microstructure giving quite fine grain sizes. For the case of the Al 7075 alloy, the alloying elements (Zn, Mg and Cu) and precipitates pin grain boundaries, which stabilize the microstructure avoiding recrystallization during processing and T6 treatment.

The microstructure corresponding to the Al 1050 (H) in the ADH19-T6 laminate shows an unusual grain growth (**Fig 2a**). It is interesting to note that the as-received lamellar structure and the rolling texture have disappeared for the Al 1050 (**Fig 2a**). A change in texture of the Al 1050 layers indicates that discontinuous recrystallization has occurred during the thermo-mechanical processing. It is known that discontinuous recrystallization can result in the preferred growth of grains of minor texture components, which dominate the final texture [15]. Additionally, the elongated grains remained in the Al 1050 close to the interface (**Fig 2a**) is a result of the diffusion of alloying elements across the interface (from the Al 7075 to the Al 1050) preventing grain growth. **Fig 2b** shows a colour gradient in the Al 1050 grain close to the interface. This result suggests that the microstructure is still made up of dislocation structures and cells with LABs due to the pinned substructure by the element diffusion. Thus, the microstructural changes observed on the constituent alloys due to the rolling process will contribute to the improvement of the intrinsic toughness. Al 7075 layers with finer grain size will present higher strength, while recrystallized Al 1050 layers will be more ductile, making difficult the crack propagation and renucleation.

In order to characterize the mechanical properties of the multilayer material, we performed Charpy impact test. The results of the Charpy impact test are reported in **Table 1**. The Charpy V-notched (CVN) energy average value for the monolithic Al 7075-T6 (D) was 62 kJ/m^2 and for the Al 1050-H24 (H) was 333 kJ/m^2. The laminate material possesses significantly higher impact energy (1095 kJ/m^2) than their

corresponding constituent materials. The absorbed energy value for the ADH19-T6 laminate in the crack arrester orientation is 17.7 times higher than that for the Al 7075 alloy and 3.3 times than that for the Al 1050. This outstanding result is much higher than that obtained in a previous work [11], and it suggests that the increase in toughness is due to the highest strength laminate constituted mainly by Al 7075 (intrinsic toughening mechanism), and extrinsic fracture mechanisms operating in the interfaces. **Figure 3** shows a SEM micrograph of a Charpy tested sample where the delamination extrinsic mechanism between every interface is clearly observed. The delamination length determines the load and plastic deformation needed for renucleating a new crack. Hence, longer delaminations increase the damage tolerance and fracture absorbed energy. Therefore, if energy absorption is the goal, tough bonds are not ideal and some controlled delamination is desirable.

In order to quantify the mechanical strength of interfaces, which are the main responsible of the damage tolerance improvement observed, shear tests along them have been performed (**Figure 4**). The interfaces in the laminate are labelled by numbers indicating their location in the laminate (for example, i4 means interface four from the surface). For comparison, monolithic as-received Al 1050 (H) and Al 7075 (D) are also included. The maximum shear stress of the Al 7075 is 261 MPa (scaled on the right ordinate axis), and the plastic shear deformation is 0.6. In contrast, the maximum shear stress of the Al 1050 is only 58 MPa, but it is much more ductile ($\gamma_{plast.max.}$=6.5). Regarding the ADH19-T6 laminate, their interfaces are more ductile than the Al 7075 and less than the Al 1050, with values of plastic shear deformation to failure between 1.2 and 5. In general, the maximum shear strengths are higher than that for the Al 1050, which is due to the reinforcement close to the interface by alloying diffusion and precipitation hardening. Shear strength requirements for bonds in aircraft structures are generally much lower (~10-20 MPa) than those observed in the present work being higher than 55MPa [16]. The shear toughness of the interfaces was measured as the area under the load-displacement curve. Values between 21-24 kJ/m^2 (i2 and i4) and 76-92 kJ/m^2 (i6, i8 and i10) were found, being for some interfaces considerably lower than the shear toughness for its constituent materials (88 and 121 kJ/m^2 for the Al 7075 and Al 1050 respectively). Comparing with previously processed laminates [11], in which similar volume fraction of high strength Al 7075 and Al 1050 was considered, the high plasticity of the Al 1050 at the processing temperature and its easiness to flow across the interface led to higher bonding degree between aluminium layers, obtaining more tough interfaces (80-120 kJ/m^2), being less prone to delamination. Previous results [17] predicted that crack goes through the interface if the interface toughness exceeds about 1/4 of the toughness of the material across the interface. Therefore, and according

to this relation, the ADH19-T6 laminate presents some interfaces prone to delamination, contributing to the high impact toughness obtained.

Summarizing, a high strength 19 layer composite laminate comprising Al 7075 (82 v%) alternated with Al 1050 (12 v%) has been developed, resulting in coarse-grained (Al 1050) and fine-grained layers with a rolling texture (β-fibre) (Al 7075). The Al 1050 layers reveal that discontinuous recrystallization has occurred. The microestructural changes observed in the constituent alloys induced by the rolling process contributed to the increase in intrinsic toughness. The laminate impact toughness was outstanding, being eighteen times higher than that for the as-received Al 7075. This noticeable damage tolerance improvement is mainly due to the high volume fraction of Al 7075 present in the laminate and extrinsic fracture mechanisms, such as crack deflection at interfaces prone to delamination.

Financial support from CICYT (Project MAT2003-01172 and MAT2006-11202) is gratefully acknowledged. C.M. Cepeda-Jiménez thanks the CSIC for a I3P contract. We also thank F.F. González-Rodríguez for assistance during hot rolling and J. Chao-Hermida for assistance with the Charpy impact test.

References

1. Aluminium. Properties and Physical Metallurgy, J.E. Hatch (Ed.), American Society for Metals, Ohio,1984.
2. B.A. Movchan, F.D. Lemkey. Mater. Sci. Eng. A 224 (1997) 136-145.
3. B.C. Kang, H. Y. Kim, O. Y. Kwon, S. H. Hong. Scripta Mater., 57 (2007) 703-706.
4. S. Bueno, C. Baudín. Key Eng. Mater. 333 (2007) 17-26.
5. F. Carreño, J. Chao, M. Pozuelo, O.A. Ruano, Scripta Mater. 48 (2003) 1135-1140.
6. M. Pozuelo, F. Carreño, M. Carsí and O.A. Ruano. Int. J. Mater. Res. (formerly: Zeitschrift fuer Metallkunde), 1 (2007) 47-52.
7. D.R. Lesuer, C.K. Syn, O.D. Sherby, J. Wadsworth, J.J. Lewandowski, W.H. Hunt Jr, Int. Mater. Rev. 41 (5) (1996) 169-197.
8. M.Z. Quadir, A. Wolz, M. Hoffman, M. Ferry. Scripta Mater. 58 (2008) 959-962
9. Ai-Ying Chen, Dong-Feng Li, Jun-Bao Zhang, Hong-Wei Song, Jian Lu. Scripta Mater. 59 (2008) 579-582.
10. C.M. Cepeda-Jiménez, M. Pozuelo, J.M. García-Infanta, O.A. Ruano, F. Carreño. Mater. Sci. Eng. A 496 (2008) 133-142.

11. C.M. Cepeda-Jiménez, M. Pozuelo, O.A. Ruano, F. Carreño. Mater. Sci. Eng. A 490 (2008) 319-327.
12. Dieter GE. Mechanical Metallurgy. McGraw-Hill, London UK, 1988, pp.12-15.
13. C.M. Cepeda-Jiménez, R.C. Alderliesten, O.A. Ruano, F. Carreño. Compos. Sci. Technol. 69 (2009) 343-348.
14. M.Z. Quadir, O. Al-Buhamad, L. Bassman, M. Ferry. Acta Mater. 55 (2007) 5438-5448.
15. F.J. Humphreys, M. Hatherly. Recrystallization and related annealing phenomenon. 2nd ed. Elsevier; 2004.
16. Y. Huang, N. Ridley, F.J. Humphreys, J.-Z. Cui. Mater. Sci. Eng. A266 (1999) 295-302.
17. J.W. Hutchinson, A short Course on: the Integrity of Thin Films and Multilayers. National University of Singapore, Singapore, 1997, p.21.

Figure Captions

Figure 1. Backscattered electron micrographs and EBSD maps showing the microstructure and microtexture of (**a** and **c**) the as-received Al 1050-H24 (H) and (**b** and **d**) Al 7075-T6 (D) in the ND-RD section.

Figure 2. EBSD maps showing the microstructure and microtexture of the ADH19-T6 laminate in the ND-RD section.

Figure 3. SEM micrograph of a Charpy fractured sample of the ADH19-T6 laminate tested in crack arrester orientation.

Figure 4. Shear tests at the interfaces of the ADH19-T6 laminate compared with as-received aluminium alloys.

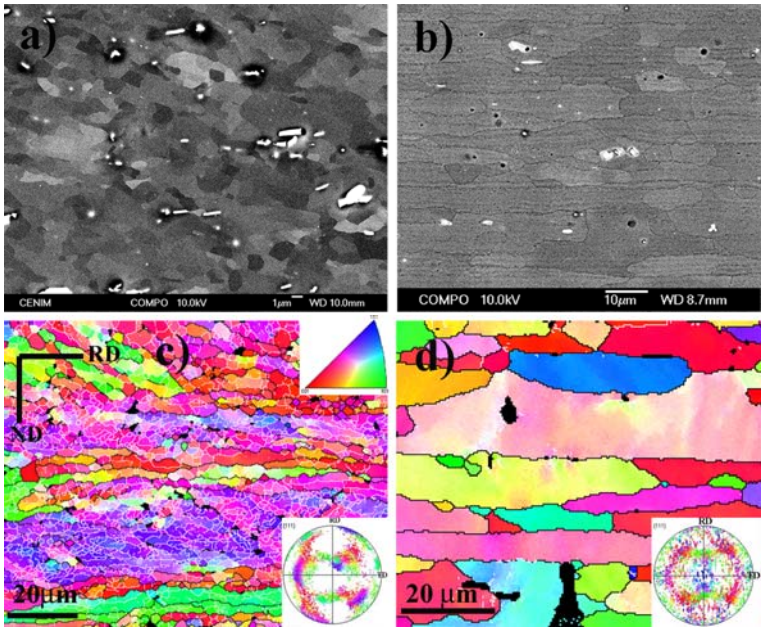

Figure 1

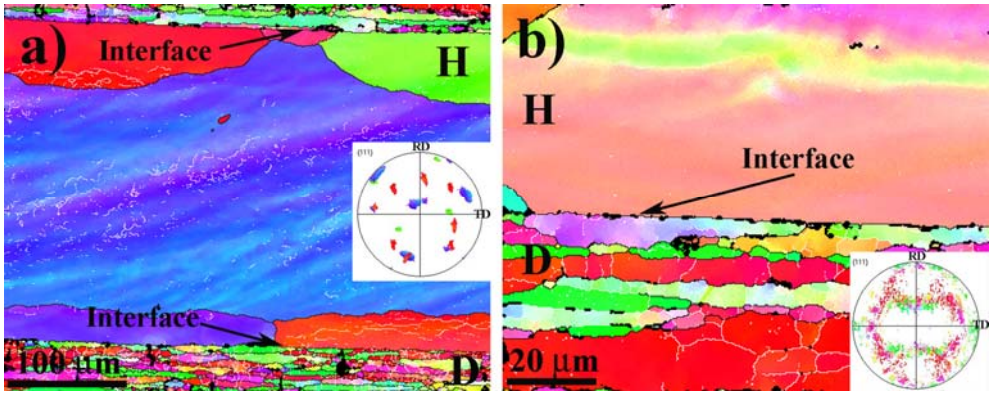

Figure 2

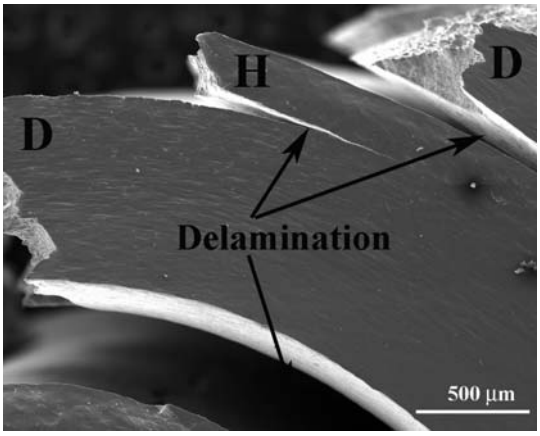

Figure 3

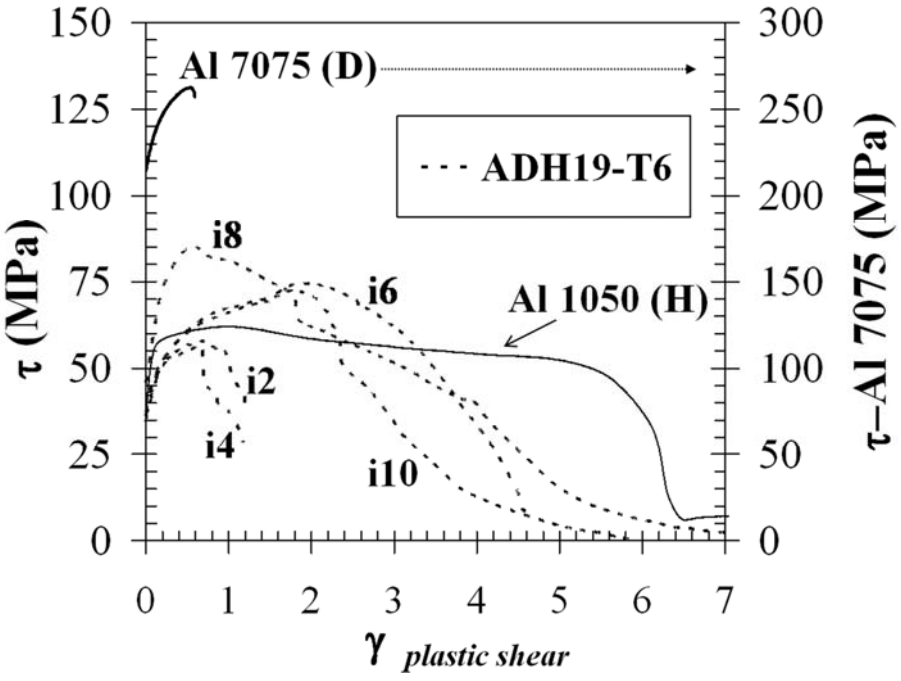

Figure 4